JOURNAL OF SPACECRAFT AND ROCKETS
Vol. 38, No. 5, September–October 2001

Computational Fluid Dynamics Analysis of a Missile with Grid Fins

James DeSpirito,* Harris L. Edge,* Paul Weinacht,† and Jubaraj Sahu†
U.S. Army Research Laboratory, Aberdeen Proving Ground, Maryland 21005-5066
and
Surya P. G. Dinavahi‡
Mississippi State University, Starkville, Mississippi 39762

An approach for using viscous computational fluid dynamic simulations to calculate the flowfield and aerodynamic coefficients for a missile with grid fins is presented. A grid fin is an unconventional lifting and control surface that consists of an outer frame supporting an inner grid of intersecting planar surfaces of small chord. The calculations were made at a Mach number of 2.5 and several angles of attack for a missile without fins, with planar fins, and with grid fins. Comparing the computed aerodynamic coefficients for the missile and individual grid fins against wind-tunnel measurement data validated the results. Very good agreement with the measured data was observed for all configurations investigated. For the grid fin case, the aerodynamic coefficients were within 6.5% of the wind-tunnel data. The normal force coefficient on the individual grid fins was within 11% of the test data. The nonlinear behavior of the normal force on the leeward fin at higher angles of attack was also accurately predicted.

Nomenclature

A	=	cell face area, m^2
C_m	=	pitching moment coefficient based on missile base area and diameter
C_p	=	pressure coefficient
C_x	=	axial force coefficient based on missile base area
C_z	=	normal force coefficient based on missile base area
D	=	missile base diameter, m
E	=	total energy, J
$\boldsymbol{F}$	=	inviscid flux vector
$\boldsymbol{G}$	=	viscous flux vector
$\boldsymbol{H}$	=	vector of source terms
$\boldsymbol{i}, \boldsymbol{j}, \boldsymbol{k}$	=	Cartesian unit vectors
M	=	Mach number
p	=	pressure, N/m^2
$\boldsymbol{q}$	=	heat flux vector
u, v, w	=	velocity components in x, y, z directions
V	=	cell volume, m^3
$\boldsymbol{v}$	=	velocity vector, $u\boldsymbol{i} + v\boldsymbol{j} + w\boldsymbol{k}$
$\boldsymbol{W}$	=	vector of conservative variables
x, y, z	=	axial, horizontal, and vertical body axes
α	=	angle of attack
ν	=	kinematic viscosity, m^2/s
ρ	=	density, kg/m^3
$\boldsymbol{\tau}$	=	viscous stress tensor

Introduction

THE U.S. Army Research Laboratory (ARL) is using computational fluid dynamics (CFD) to investigate the aerodynamic characteristics and flowfield structure of grid fins, also known as lattice controls. A grid fin is an unconventional lifting and control surface that consists of an outer frame supporting an inner grid of intersecting planar surfaces of small chord. Grid fins have been employed on some Soviet missiles but have not been included on any missile systems in the west.[1] Interest in grid fins is primarily geared toward their potential use on highly maneuverable munitions due to their advantages over conventional planar controls at high angles of attack and high Mach number.

The aerodynamics of grid fins have been investigated since 1985 by U.S Army Aviation and Missile Research and Development Center, Huntsville, Alabama.[2–4] These investigations indicated that grid fins have some advantages over conventional, planar fins. One advantage is the ability to maintain lift at higher angles of attack because grid fins do not have the same stall characteristics of planar fins. Another advantage is the very small hinge moment, which can reduce the size of control actuator systems. Because curvature of the grid fins had little effect on their performance, folding down the fins onto the missile body is a storage design advantage. The main disadvantage was higher drag than that of planar fins, although techniques for minimizing drag by altering the grid fin frame cross-sectional shape were demonstrated.[3] These studies also showed that grid fins experience a loss in control effectiveness in the transonic regime due to flow choking in the individual cells.

The Defence Evaluation and Research Agency (DERA), United Kingdom, has performed wind-tunnel tests on grid fins and compared their aerodynamic characteristics to conventional planar fins.[1] These studies confirmed some of the previous results and showed improved yaw stability due to the ability of the grid fins to generate side force. The results also showed that the vertical fins contribute about 30% of the static longitudinal stability when oriented in the cruciform (+) configuration.

Aeroballistic range flight tests have recently been conducted at the U.S. Air Force Research Laboratory Aeroballistic Research Facility, Eglin Air Force Base, Florida.[5] These subscale free-flight tests were the first reported for a missile configuration with grid fins. In addition to providing the raw data to derive the aerodynamic coefficients for the grid fin models, shadowgraphs of the models in flight at Mach numbers between 0.39 and 1.65 showed an interesting shock structure in and around the fins.

There have also been theoretical and numerical methods used to estimate the lift characteristics of grid fins. Methods have been developed for the subsonic (vortex lattice theory), transonic (empirical methods), and supersonic (Evvard's theory) regimes (see Refs. 6–10). Empirical extensions were used to gain data for missiles at large angles of attack. If body upwash terms are included, these methods provide adequate aerodynamic characteristics of grid fins for preliminary design purposes in the subsonic and supersonic regimes.

Received 16 December 1999; presented as Paper 2000-0391 at the AIAA 38th Aerospace Sciences Meeting, Reno, NV, 10–13 January 2000; revision received 10 July 2001; accepted for publication 12 July 2001.

*Aerospace Engineer, Weapons and Materials Research Directorate, Ballistics and Weapons Concepts Division. Senior Member AIAA.

†Aerospace Engineer, Weapons and Materials Research Directorate, Ballistics and Weapons Concepts Division. Associate Fellow AIAA.

‡Onsite Computational Fluid Dynamics Lead, U.S. Army Research Laboratory Major Shared Resource Center Programming Environment and Training Program; currently Systems Engineer, Platform Computing, Inc., Millersville, MD 21108. Senior Member AIAA.

The first reported CFD calculations made on grid fins were sponsored by the Defence Research Establishment Valcartier, Canada.[11–13] These studies only included inviscid (Euler) simulations. The authors concluded that the inviscid CFD calculations provided a reliable means of studying the flows past missiles with grid fins. Comparisons with data[4] showed reasonable agreement for the fin normal force. The Euler calculations for the grid fins compared better with the measured data than Euler calculations for the planar fins. The authors attributed this to the shorter surfaces of the grid fins in the axial direction, as compared to planar fins.[12] The results of the viscous calculations from the present study help to explain this effect. Another study involving inviscid computations[14] concentrated on the flow in the region of the grid fin while studying the effect of a fairing ahead of the base of the fin. These investigations were performed at Mach numbers of 1.5–2.5.

This paper presents the results of the first viscous CFD calculations made involving a missile with grid fins. The results are validated by comparing them against wind-tunnel data.[1] Simulations of the missile body alone and with planar fins were also performed as part of the validation process.

Numerical Approach

The investigation involved using CFD to determine the flowfield and aerodynamic coefficients on a 13-caliber, four-finned, generic missile shape (Fig. 1). The missile has a 3-caliber tangent ogive, and the fin pitch axis is located 1.5 diameters before the aft end of the missile. The analysis proceeded in three steps. The first involved the missile without fins, case B1A (Fig. 1, top); the second was with the missile with planar fins, case B1AC2R (Fig. 1, middle); and the third was the missile with a set of grid fins, case B1AL2R (Fig. 1, bottom). The configurations were labeled according to the designations used at DERA.[1] The span and chord of the planar fin were 1.0 caliber. The span of the grid fin was 1.1 caliber and the chord was 0.17 caliber. All analyses were performed at $M = 2.5$ and at a minimum of three angles of attack: 0, 10, and 20 deg. The simulations were performed with the missile in the cruciform (+) configuration, and symmetry (x–z plane) was used so that only a half-plane was modeled.

Steady-state calculations were made to compute the flowfield for the three cases using the commercial CFD code, FLUENT version 5.1. The implicit, compressible (coupled), unstructured-grid solver was used. The three-dimensional, time-dependent, Reynolds-averaged Navier–Stokes equations are solved using the finite volume method:

$$\frac{\partial}{\partial t}\int_V \boldsymbol{W}\,\mathrm{d}V + \oint [\boldsymbol{F} - \boldsymbol{G}]\cdot \mathrm{d}\boldsymbol{A} = \int_V \boldsymbol{H}\,\mathrm{d}V \tag{1}$$

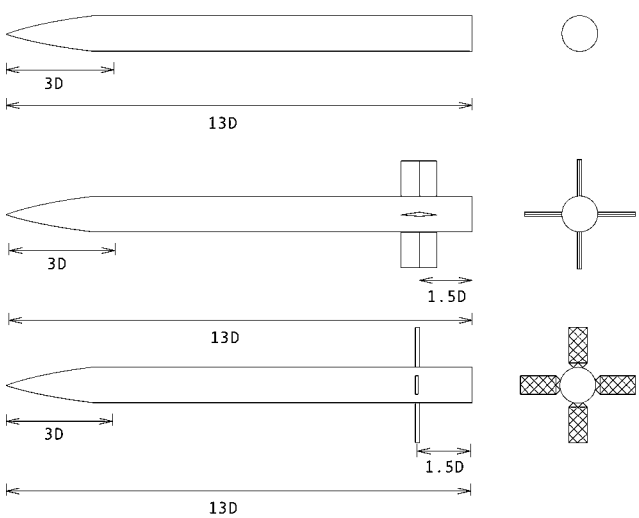

Fig. 1 Basic missile shape with no fins (B1A, top), planar fins (B1AC2R, middle), and grid fins (B1AL2R, bottom).

where

$$\boldsymbol{W} = \begin{Bmatrix} \rho \\ \rho u \\ \rho v \\ \rho w \\ \rho E \end{Bmatrix}, \quad \boldsymbol{F} = \begin{Bmatrix} \rho \boldsymbol{v} \\ \rho \boldsymbol{v} u + p\boldsymbol{i} \\ \rho \boldsymbol{v} v + p\boldsymbol{j} \\ \rho \boldsymbol{v} w + p\boldsymbol{k} \\ \rho \boldsymbol{v} E + p\boldsymbol{v} \end{Bmatrix}, \quad \boldsymbol{G} = \begin{Bmatrix} 0 \\ \boldsymbol{\tau}_{xi} \\ \boldsymbol{\tau}_{yi} \\ \boldsymbol{\tau}_{zi} \\ \boldsymbol{\tau}_{ij} v_j + \boldsymbol{q} \end{Bmatrix} \tag{2}$$

The inviscid flux vector $\boldsymbol{F}$ is evaluated by a standard upwind flux-difference splitting. In the implicit solver, each equation in the coupled set of governing equations is linearized implicitly with respect to all dependent variables in the set, resulting in a block system of equations. A block Gauss–Seidel, point implicit linear equation solver is used with an algebraic multigrid method to solve the resultant block system of equations. The coupled set of governing equations is discretized in time and time marching proceeds until a steady-state solution is reached. In the implicit scheme, which was used in this study, an Euler implicit discretization in time is combined with a Newton-type linearization of the fluxes.

The Spalart–Allmaras,[15] one-equation turbulence model was used for these calculations. In FLUENT, the original version of the Spalart–Allmaras model is modified to allow the use of wall functions when the mesh resolution is not sufficiently fine to resolve the viscous-affected, near-wall region of the boundary layer.[16] This capability was used in generating the mesh so that the computational requirements were reduced as much as possible. Second-order discretization was used for the flow variables and the turbulent viscosity equation.

The geometry and unstructured meshes for the three configurations were generated using the preprocessor, GAMBIT, supplied in the FLUENT software suite. In generating the meshes, boundary-layer mesh spacing was used near the missile body and fin surfaces. Advantage was taken of the wall function option of the solver in FLUENT, and the first point off the surface (cell center) was about 0.002 caliber. All mesh stretching was kept below a ratio of 1.2. Hexahedral cells were used except for a small region ahead of and partly over the first 0.1 caliber of the nose of the missile (1% of the total length). The latter region was made up of tetrahedrons and pyramid transition elements. The tetrahedral mesh was made to cover a small part of the missile nose to allow a transition from the missile nose to the freestream part of the mesh ahead of the missile. This approach was used because of a limitation in GAMBIT, which was removed in a later release of the software. Therefore, a true boundary-layer-type mesh was not covering the first 1% of the missile body, but this had no observable effect on the results. The B1A case was meshed as five separate volumes, one in the freestream region, two over the first 10 calibers of the missile, and two over the last 3 calibers. This methodology was used so that the mesh in the first two regions could be used regardless of the fin type. The meshes between volumes were conformal, or exactly matching at the boundary surfaces. The total number of cells in this case was about 670,400. The mesh for the planar fin case was modified slightly so that only one volume covered the first 10 calibers of the missile. The tail region consisted of seven volumes located ahead of, behind, and between the fins and off the fin tips. The total number of cells for this case was about 1.2×10^6, and again the mesh was totally conformal.

The geometry for the grid fin case is shown in Fig. 2. The solid modeling capabilities of GAMBIT simplified the generation of the grid fin geometry. In the wind-tunnel model, the frame of the grid fin is chamfered to reduce drag.[3] A chamfer was not included in the geometric model used in the FLUENT calculations so that mesh generation could be simplified. The mesh for the freestream region and the first 10 calibers of the missile body was similar to that for the planar fin case. Because of the complexity of the mesh in the region around the grid fins, and to minimize the total mesh size, a nonconformal mesh interface was used on an axial plane 10 calibers from the nose. With this type of interface, which is used in FLUENT to handle sliding meshes, the cells on either side of the interface are treated as general polyhedrons, instead of tetrahedrons or, as in this case, hexahedrons. Some interface cells will then have more than one face shared with a neighboring cell on the other side of the interface. For

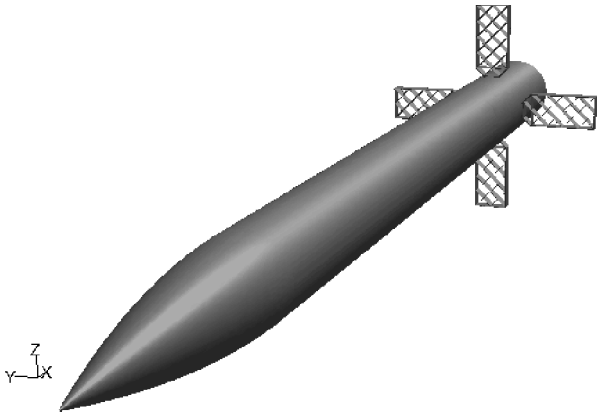

Fig. 2 Geometry for grid fin case (B1AL2R).

the purpose of computing the gradient at the cell center, the face values are taken to be the average of the cell values neighboring the face. Accuracy will be compromised if the cells at the interface are highly skewed or if there is a large cell size variation across the interface.

In the mesh used in this study, the hexahedral cells at the interface are not skewed, but the variation of the cell size across the interface was larger than optimum. The interface was located 10 calibers from the nose and 1.5 caliber forward of the fins. The effect of any inaccuracy due to the nonconformal interface is believed small because the aerodynamic coefficients compared very well with experimental data and little effect on the flowfield was observed. The calculation of the crossflow separation region on the leeward side of the missile, which flows through this interface, is also believed accurate. This is shown by the accurate prediction of the normal force on the leeward grid fin, which is very sensitive to the flow in the crossflow separation region. The total number of cells in this mesh was about 3.2×10^6, with 2.5×10^6 in the fin region (10–13 calibers). The fins, interior cells, and the thin region circumferentially between the fins were meshed first. The surface mesh was then projected axially forward and rearward with smoothing. There were one or two cells across the front and rear of the grid fin web and frame surface. This dimension is the same order of magnitude as the first cell spacing off the surface (0.002 caliber).

The base flow was not simulated in these calculations, so that the mesh stopped at the end of the missile. The computational domain extended 4 calibers from the missile body. About 72 cells were used on the missile body in the circumferential direction, with this value increased in the fin region. An outflow boundary condition was used downstream, a pressure inflow (freestream conditions) boundary condition was used upstream, and a far-field pressure (nonreflecting) boundary condition was used for the outer boundary. A nonslip wall boundary condition was used for all solid surfaces. The y^+ value was about 40–60 along the missile body, which is optimum for wall functions. The maximum value was about 150 along the ogive and between 100 and 140 on the grid fin surfaces. The Reynolds number was 13.1×10^6 m^{-1}, or 1.2×10^6 for this model. The freestream temperature and pressure were 137 K and 8325 Pa, respectively.

The FLUENT simulations were performed in parallel using four to six processors on a Silicon Graphics Onyx 2 with R12000 processors. The number of processors was limited by the software license in place at the time. The solutions were started with a Courant–Friedrich–Lewy (CFL) number of either 1.0 or 2.0. The CFL number was quickly increased to 4.0 or 5.0 for the remainder of the run. The grid fin calculations took about 4.5–5 min/iteration using six processors. Convergence was determined by tracking the change in the aerodynamic coefficient values and the flow residuals during the solution. The aerodynamic coefficients converged in about 600 iterations. It took about 1500 iterations for the turbulent viscosity to converge, with the scaled residual reduced to about 10^{-6}. A grid sensitivity study was not performed due to the complexity of the grid fin geometry and time constraints. The mesh spacing on the missile surfaces and the extent of the computational domain were based on those used in previously validated missile and projectile simulations performed at ARL.[17]

The no fin and planar fin cases were also run with a structured-mesh, finite difference code, ZNSFLOW,[17] which solves the complete set of three-dimensional, time-dependent, Reynolds-averaged, thin-layer, Navier–Stokes equations in generalized coordinates. The time-dependent equations are solved via a time-iterative solution technique to obtain the final steady-state converged solution. The time-marching technique applied is an implicit, partially flux-split,[18] upwind numerical scheme.[19,20] The aerodynamic coefficients calculated with this code using the Baldwin–Lomax turbulence model are presented in the next section, along with those calculated with FLUENT. Because ZNSFLOW does not use wall functions in the turbulence models, the first grid point off the solid surfaces was about 5×10^{-6} calibers, giving a y^+ value of approximately 1. The computational domain was the same, and the mesh spacing on the missile surfaces was similar to that used in the FLUENT calculations. A multiblock or zonal grid was generated using the commercial GRIDGEN code.

The ZNSFLOW code has been extensively validated for projectile and missile geometries over the past decade, including body-alone and planar fin configurations. The ZNSFLOW calculations have been included to provide an additional means of assessing the FLUENT code results, especially in light of the unstructured meshing and turbulence modeling with wall functions employed in FLUENT. The ZNSFLOW code also has a chimera overset gridding[21] capability that was initially considered for application to the grid fin configuration. However, the FLUENT code was applied to the grid fin configuration because the geometry was already created using the GAMBIT preprocessor, and it was believed that mesh generation would be faster using GAMBIT. The application of chimera overset grids to the grid fin configuration is seen as a worthwhile research objective; however, it is beyond the scope of the current effort.

A series of inviscid calculations was also made on the grid fin configuration. These simulations used the same geometry as the viscous calculations, except for the fin–body interface, where a short circular stem was used for mesh generation purposes. The chamfer on the grid fin frame was also included. A Cartesian mesh solver, TIGER,[22,23] and automatic mesh generation program, CART3D,[24,25] were used for the inviscid simulations. The Cartesian flow solver integrates the finite volume form of the Euler equations to steady state using a multistage Runge–Kutta time integration procedure.[22] The mesh generation and solution time were much less than the time required for the viscous calculations. The Cartesian grid had about 1.3×10^6 grid points, and the turnaround time was less than a day. The calculations for the flow solver were carried out on a Sun E10K machine on a single CPU. The flow solver took about 20 μs/cell/iteration and typically needed about 1500 iterations for convergence. The aerodynamic coefficients calculated with the inviscid simulations are compared to the viscous calculations in the following section.

Results and Discussion

Aerodynamic Coefficients

When the computed flowfields were used, the viscous and pressure forces were integrated along the missile body and fin surfaces to calculate the aerodynamic coefficients. The normal force, axial force, and pitching moment coefficients are presented in missile-based coordinates, a right-handed system with the x axis coinciding with missile axis, positive directed to the rear, and the z axis oriented upward. The pitching moment is expressed about the nose of the missile. The reference area is the cross-sectional area of the missile base, and the reference length is the diameter of the missile. The calculated coefficients are compared to wind-tunnel measurements performed at DERA.[1] Forebody axial force data were obtained by correcting the measured axial force for the base drag component using measured pressures obtained at the base of the model. The repeatability of the DERA data was reported to be within 1% at 2.5 Mach over the range of α investigated.[1]

Body-Alone Case

The aerodynamic coefficients for the body-alone case B1A calculated from the FLUENT and ZNSFLOW solutions are shown in

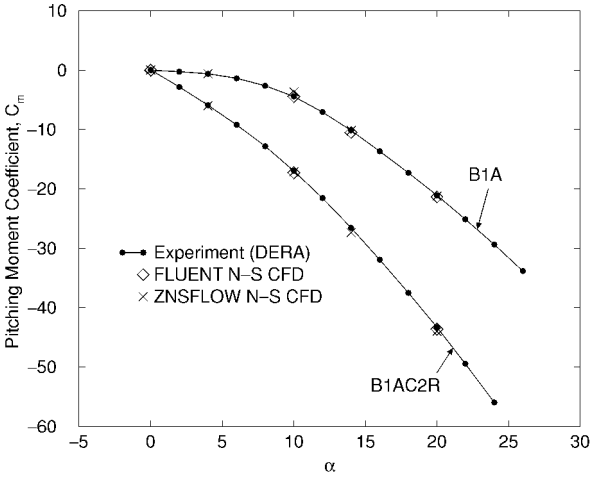

Fig. 3 Pitching moment coefficient vs α (deg) for B1A and B1AC2R cases.

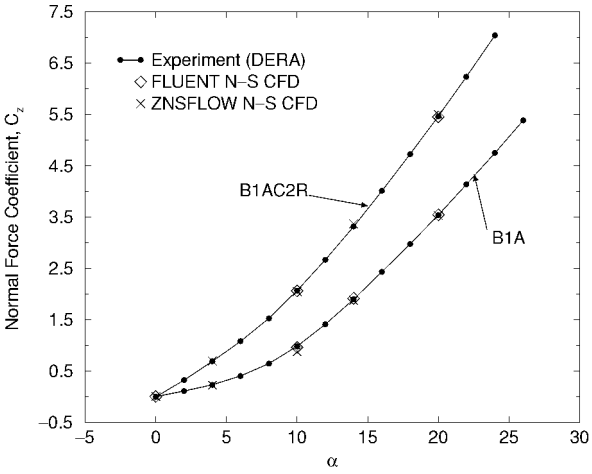

Fig. 4 Normal force coefficient vs α (deg) for B1A and B1AC2R cases.

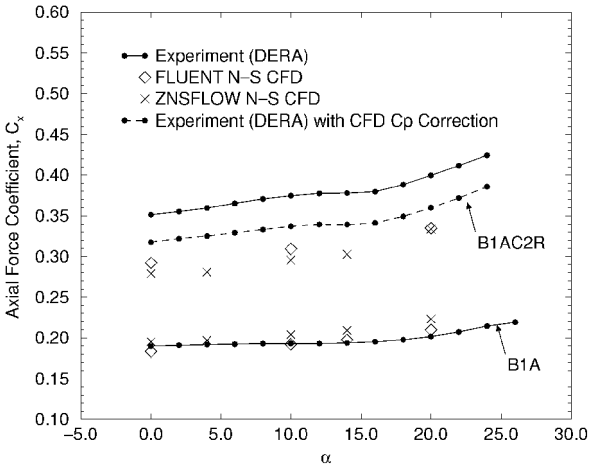

Fig. 5 Axial force coefficient vs α (deg) for B1A and B1AC2R cases.

Figs. 3–5. Data from DERA wind-tunnel measurements are also shown. The calculated C_m, C_z, and C_x are shown at $\alpha = 0$, 10, 14, and 20 deg for the FLUENT calculations and at 0, 4, 10, 14, and 20 deg for the ZNSFLOW calculations. The calculated results show very good agreement with the measured aerodynamic coefficients. The maximum difference between the FLUENT predictions and the measured C_m was 3.6%, with the maximum occurring at $\alpha = 14$ deg. With the exception of an 18% difference between the ZNSFLOW prediction and the experiment at $\alpha = 10$ deg, the ZNSFLOW and FLUENT results compared well with the measured C_m. The maximum difference between the FLUENT predictions and the measured C_z was 2.0%, with the maximum occurring at $\alpha = 10$ deg. Similar to the C_m results, a 10% difference between the ZNSFLOW predictions and the measured C_z was found at $\alpha = 10$ deg, although much better comparisons were found at the other angles of attack. The maximum difference between the FLUENT predictions and the measured C_x was 4.2%, with the maximum occurring at $\alpha = 20$ deg. The ZNSFLOW predictions followed the same trend of increasing C_x with α, with a 12% difference between the predicted and measured C_x at $\alpha = 20$ deg. The difference calculation did not include the $\alpha = 0$ deg case for C_m and C_z because these parameters are nominally zero at this angle of attack.

Planar Fin Case

The aerodynamic coefficients for the planar fin case B1AC2R calculated from the FLUENT and ZNSFLOW solutions are also shown in Figs. 3–5 as a function of α. The calculated coefficients are shown at $\alpha = 0$, 10, and 20 deg for the FLUENT calculations and at 0, 4, 10, 14, and 20 deg for the ZNSFLOW calculations. The calculated C_z and C_m again show very good agreement with the measured aerodynamic coefficients. The maximum difference between the FLUENT predictions and the measured C_m was 1.8%, with the maximum occurring at $\alpha = 10$ deg. The maximum difference between the ZNSFLOW predictions and the measured C_m was 3.1%, with the maximum occurring at $\alpha = 14$. The maximum difference between the FLUENT predictions and the measured C_z was 0.2%, with the maximum occurring at $\alpha = 10$ deg. The maximum difference between the ZNSFLOW predictions and the measured C_z was 1.5%, with the maximum occurring at $\alpha = 14$.

The calculated values of C_x were lower than the measured values, but they predicted the same increase with α that the experimental data showed. The FLUENT predictions were within 17% of the experimental data, and the ZNSFLOW predictions were within 22%. The viscous component of the axial force was about 40% of the total (regardless of angle of attack) in the FLUENT and ZNSFLOW simulations.

Interestingly, in this case the predicted values of axial force are lower than the measured values, whereas the opposite was found for the body-alone and the grid fin cases. Some further investigation was warranted, and additional FLUENT calculations of the planar fin and body-alone models were performed with part of the wind-tunnel sting included in the model. In the wind-tunnel experiments, the total axial force acting on the force balance is measured. The pressure on the base of the missile is measured using a small number of pressure gauges (usually one or two). The C_p on the base of the wind-tunnel model is then used to remove that component of C_x from the total C_x, resulting in what is called the forebody C_x. This value is what is shown as the solid line in Fig. 5. If the measured value of the pressure on the base of the wind-tunnel model is not accurate, then forebody C_x, used to compare to the CFD, will not be accurate. It is important to have an accurate measure of the forebody axial force because CFD calculations do not normally include the sting and in some cases do not include the base flow at all, as in this study. When additional CFD calculations are performed including the sting, the calculations can be compared directly to those measured by the wind-tunnel force balance, removing base pressure measurement issue. In addition, the calculation of the missile base flow will determine whether there is an effect of not calculating the base flow in the original calculations.

The results for the body-alone case with the sting were very similar to the case without the sting. There was very little change in the aerodynamic coefficients, with the forebody C_x within 5.1% for the case with the sting and within 4.2% without. The total C_x (including missile base) was within 6.4% of the experimental data for the case with the sting. These results indicate that an accurate measure of the average pressure on base of the missile was obtained in the wind-tunnel experiments because both the forebody and total C_x compare well with the CFD.

The predicted values for C_m, C_z, and forebody C_x for the planar fin case with the sting were also similar to the predictions without the sting, with the forebody C_x again being underpredicted by 14%. However, the value for the total C_x was within 4.8% of the experimental value. This result indicates that an accurate measure

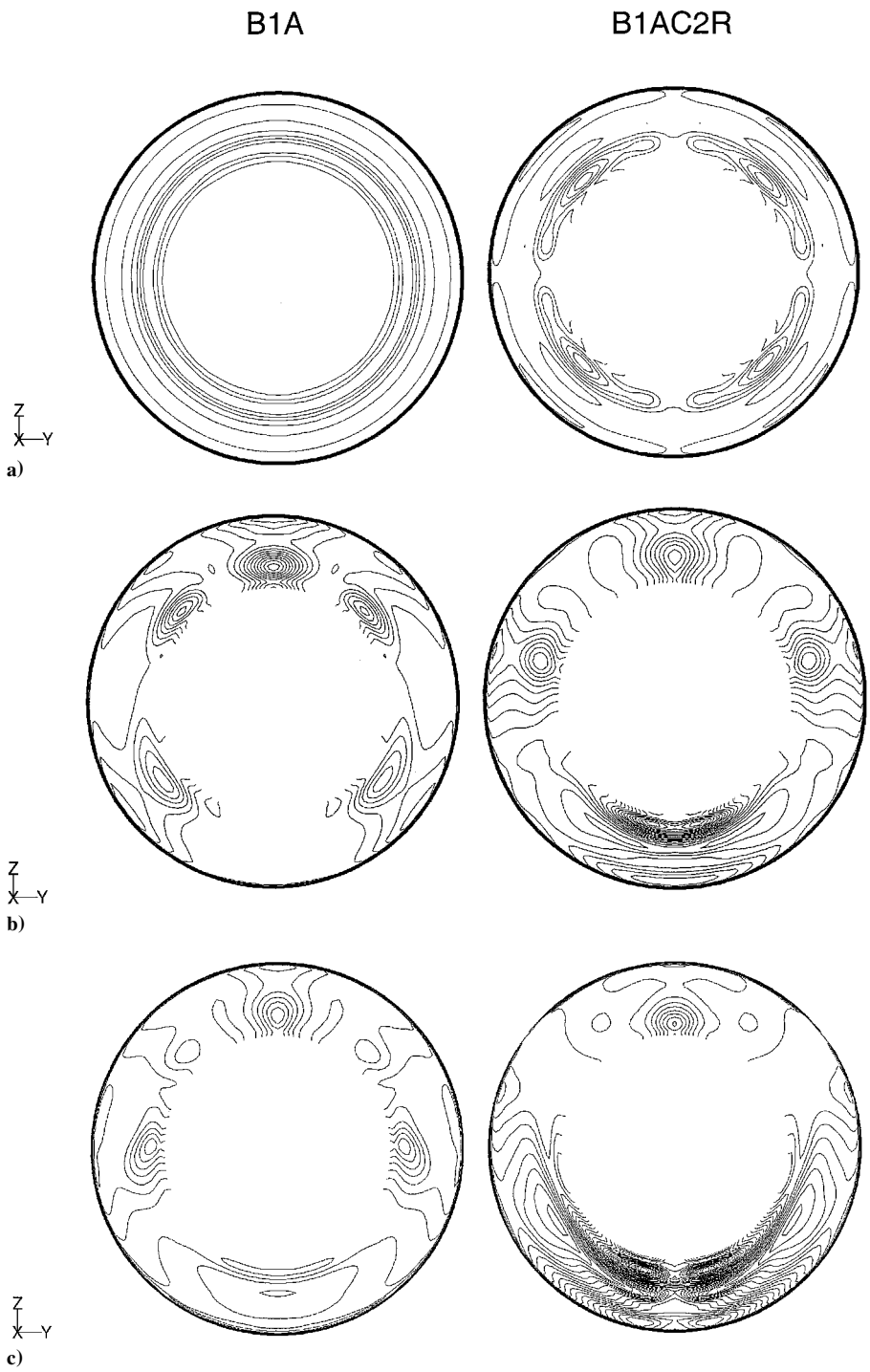

Fig. 6 Pressure coefficient on missile base with sting for a) $\alpha = 0$, b) $\alpha = 10$, and c) $\alpha = 20$ deg.

of the average pressure on the base of the missile was not achieved in the wind-tunnel experiments. Comparing contour plots of C_p on the annular base region in Fig. 6 shows that there are larger gradients and a more nonuniform distribution of pressure on the base in the planar fin case. Therefore, the measuring of pressure in only one or two locations is less likely to give an accurate determination of the average pressure on the base in planar fin case. Although the comparison of the total C_x is more accurate, the average C_p on the base of the missile from the CFD calculations, instead of the measured C_p, was used to estimate the experimental forebody C_x. These corrected data are also shown in Fig. 5, and the CFD calculations compare reasonably well, to within 4.8% of the experimental data. To summarize, the simulations with and without the sting give essentially the same results for the forebody aerodynamic coefficients. Modeling the sting allows comparison of the CFD calculations with the measured total C_x, which compared very well for both cases.

Grid Fin Case

The aerodynamic coefficients for the grid fin case B1AL2R calculated from the FLUENT and the inviscid TIGER solutions are shown in Figs. 7–9 as a function of α. The calculated coefficients are shown at $\alpha = 0$, 10, 12, and 20 deg for both CFD cases. The calculated C_z and C_m again show very good agreement with the measured aerodynamic coefficients. The maximum difference between the FLUENT predictions and the measured C_m was 6.2%, with the maximum occurring at $\alpha = 10$ deg. A portion of this difference appears to be associated with a 0-deg bias in the experimental data. Larger differences between the TIGER predictions and the measured C_m are evident, with a maximum difference of 18% at $\alpha = 12$ deg. Similar comparisons between computation and experiment were found for the force coefficient C_z. The maximum difference between computation and experiment was 6.6% at $\alpha = 10$ deg for the FLUENT predictions and 13% at $\alpha = 12$ deg for the TIGER predictions. A significant portion

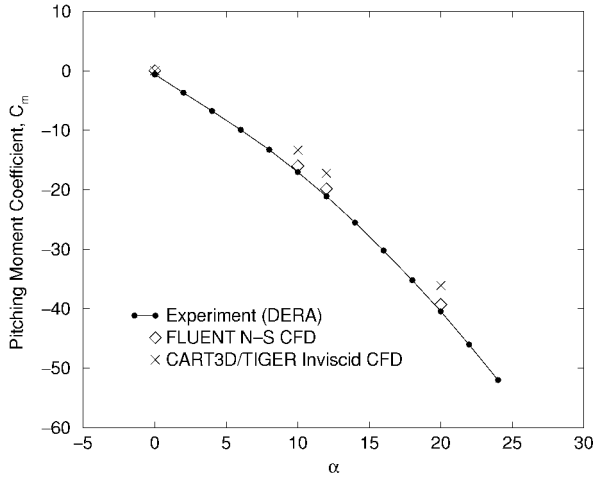

Fig. 7 Pitching moment coefficient vs α (deg) for B1AL2R case.

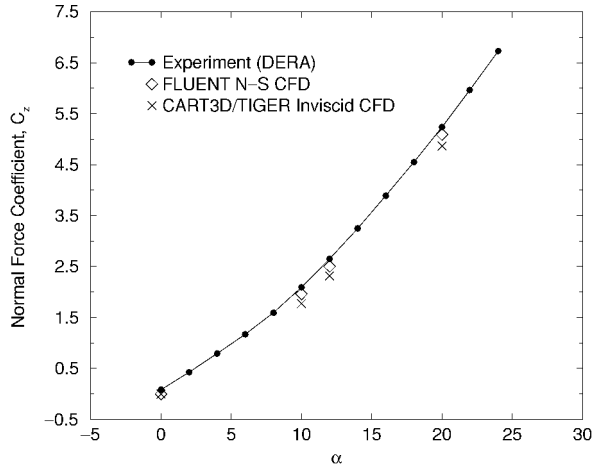

Fig. 8 Normal force coefficient vs α (deg) for B1AL2R case.

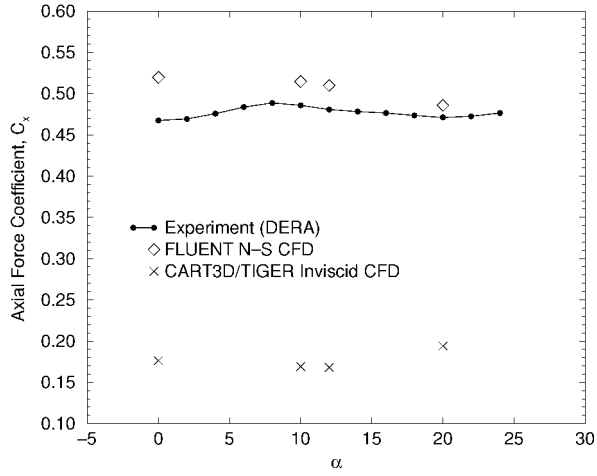

Fig. 9 Axial force coefficient vs α (deg) for B1AL2R case.

of the difference between the FLUENT predictions and the measured data appears to be related to a 0-deg bias in the measured C_z. However, the inviscid TIGER predictions consistently underpredict measured C_z.

The FLUENT axial force predictions were a little higher than the measured values, a 3–6% difference for $\alpha > 0$ and an 11% difference at $\alpha = 0$. Regardless of the angle of attack, the viscous skin-friction component of the C_x was 29%. The inviscid TIGER results appear to underpredict the measured C_x by more than the expected difference due to viscous drag. Outside the obvious differences produced by the viscous skin-friction drag, the differences in C_x between

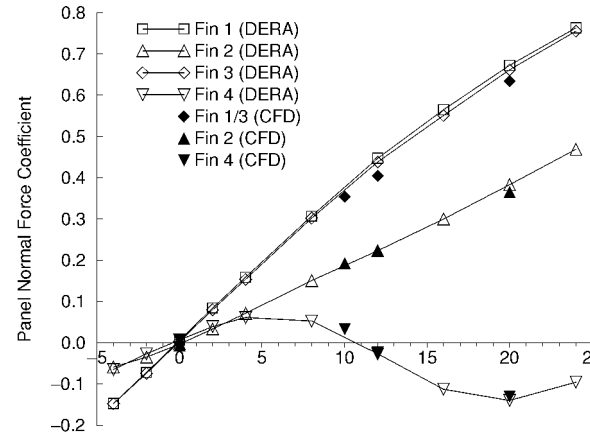

Fig. 10 Normal force coefficient vs α (deg) on individual grid fins.

the FLUENT and TIGER predictions were isolated to the grid fins themselves. Further investigation, including inviscid FLUENT predictions, revealed that some of the differences are due to modeling issues. For example, the geometry of the fins used in the TIGER and FLUENT simulations was slightly different. In the TIGER simulations, the frame of the grid fin was chamfered, as in the wind-tunnel model, which was done to reduce drag.[3] At Mach 2.5, reductions of up to 23% in the fin drag were found for the type of chamfering used on the fins in the present study.[3] Although this explains some of the differences between the FLUENT and TIGER predictions, it fails to explain the significant under prediction of fin C_x in the TIGER simulations. Subsequent inviscid calculations (M. Aftosmis, NASA Ames Research Center, private communication, October 2000) with additional grid refinement and algorithmic improvements[26] reduced the difference between the predicted and measured C_m and C_z to within 11%, but did not significantly reduce the differences in C_x.

Forces on Fins

The normal force coefficient on the individual grid fins from the FLUENT calculations are shown in Fig. 10, along with the measured wind-tunnel data as a function of α (Ref. 1). The fins are numbered 1–4, with fin 1 in the 3 o'clock position and fin 4 in the 12 o'clock position if looking forward from the rear of the missile in the + configuration. In the simulations, fins 1 and 3 are the same due to symmetry. The normal force on the fins was predicted very well, with the largest difference at about 11%. As expected, the normal force is greatest on the horizontal fins. The windward fin (fin 2, bottom) also provides a substantial normal force. The leeward fin (fin 4, top) provides a similar normal force as fin 2 up to about $\alpha = 4$ deg, but then goes nonlinear and negative at higher angles of attack. As described by Simpson and Sadler,[1] the nonlinear shape of the normal force vs α curve for the leeward fin is caused by its location in the crossflow separation region at higher α. As shown later in plots of the flowfield, the local α varies over the leeward grid fin. Some parts of the fin will be at an effective negative α, while other parts are at an effective positive α.

The normal force coefficient on the individual grid fins showed that the inviscid calculations did not accurately predict the normal force on the leeward fin. The calculated normal force coefficient was within 5.5% and 14% of the experimental data on the horizontal and windward fins, respectively. However, the normal force coefficient on the leeward fin was much larger than the experimental value, especially between $\alpha = 5$ and $\alpha = 15$ deg. At $\alpha = 10$ deg, the calculated normal force coefficient on the leeward fin was a factor of 8.4 times larger than the experimental value. As might be expected, the inviscid calculations do not capture the crossflow separation location on the leeward side of the missile as accurately as the viscous calculations. This leads to a different flow entering the leeward fin, resulting in the wrong normal force. A missile with planar fins would have no normal force contribution from the leeward fin, and so a difference would be expected when comparing the total normal force and pitching moment calculated from the inviscid solution with the experimental data. In the grid fin case, the lower normal force on the

missile body caused by the incorrect crossflow separation prediction was countered by the larger normal force on the leeward fin caused by the incorrectly predicted flowfield. It is likely a coincidence that the values were such that the overall normal force coefficient was still within 11% of the experimental data.

To confirm the result of the inviscid code, an inviscid solution was performed with FLUENT at $\alpha = 10$ deg using the same mesh as in the viscous calculations. The calculated normal force coefficient was within 1% of the experimental data for the horizontal and windward fins, whereas the normal force coefficient calculated for the leeward fin was a factor of 9 times the experimental value. These results show that one must be careful how the results of an inviscid solution are used. The Cartesian mesh generator, CART3D, which is used with the inviscid code, significantly reduced the time required for mesh generation, even for the complicated grid fin geometry. The fast grid generation method makes this code especially attractive as a design tool. However, one must be aware of the limitations of this approach, including the need for viscous corrections in the axial force and possible reduced fidelity in the predictions of the individual fin forces and moments.

The axial force coefficient on individual grid fins were about 2–3 times greater than those on the planar fins. The viscous component of the axial force on the grid fin was about 1.5 times greater than on the planar fins. Although it was speculated that the smaller chord of the grid fin might impart less viscous force than a planar fin,[12] the summation of the viscous forces on all of the lattice surfaces of the grid fin leads to higher viscous forces. The likely reason inviscid calculations of the aerodynamic coefficients on a missile with grid fins were more accurate than those for a missile with planar fins[12] is that the viscous component, as a percentage of the total axial force on the fin, is less for the grid fin case. In this study, the viscous component of the axial force on the individual grid fin was 16% of the total vs 30% for the planar fin. With a larger component of the axial force in the grid fin case due to form and wave drag, an inviscid calculation may be expected to compare better with measured data than a planar fin case.

Grid Fin Flowfield

A contour plot of C_p on the symmetry plane is shown for the $\alpha = 12$ deg case in Fig. 11. A strong oblique shock is seen emanating from the windward side of the nose, with a weaker shock coming off of the leeward side. An expansion fan is seen coming off of the ogive–body interface. A crossflow separation region, which increases with α, is observed on the leeward side of the missile. The crossflow separation region encloses the entire leeward fin at $\alpha =$ 20 deg.

There is a complex, three-dimensional shock structure emanating off of the grid fins. Figures 12–14 show C_p contours on the symmetry plane through the leeward fin at $\alpha = 10$, 12, and 20 deg, respectively. At this Mach number, the shock and expansion waves do not reflect off of the interior walls of the grid fin cells.[2] Instead, they first reflect off one another inside the grid fin cell, setting up several more reflections in the wake of the fin. The windward fin, not shown, is at a positive effective α for all cases. However, the effective α on parts of the leeward fin is negative as α for the missile changes, due to the vortices in the crossflow separation region. At $\alpha = 10$ deg (Fig. 12), the top two cells of the leeward fin are at an effective positive α, with the shock wave emanating from the top of the cell. The third cell from the top is at nearly a 0-deg α, with shock waves emanating from the top and bottom of the cell. Finally, the lower two cells are at an effective negative α, with the shock wave emanating from the bottom of the cell. At $\alpha = 12$ deg (Fig. 13), the crossflow separation region on the leeward side of the missile is larger, and now the second

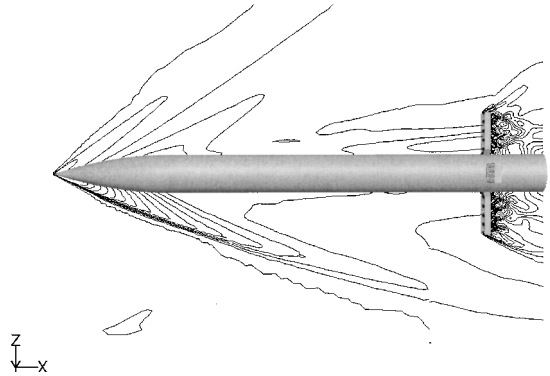

Fig. 11 Pressure coefficient on symmetry plane for grid fin case; $\alpha = 12$ deg.

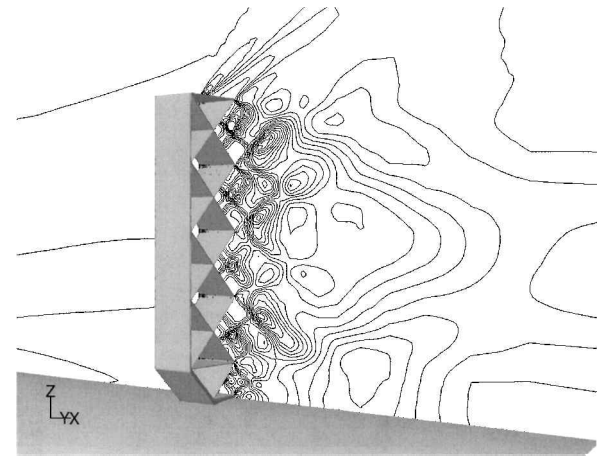

Fig. 12 Pressure coefficient contours on symmetry plane through leeward fin (fin 4); $\alpha = 10$ deg case.

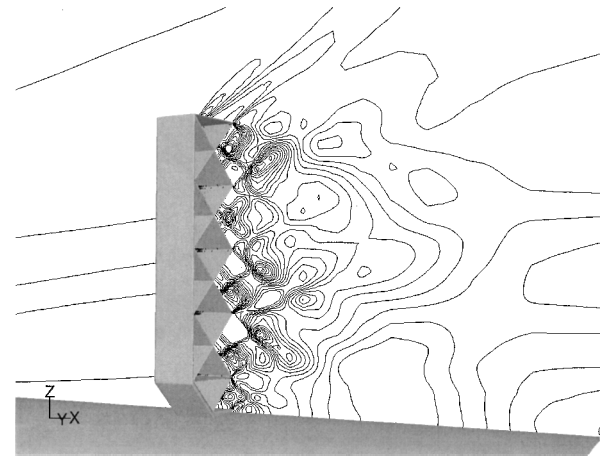

Fig. 13 Pressure coefficient contours on symmetry plane through leeward fin (fin 4); $\alpha = 12$ deg case.

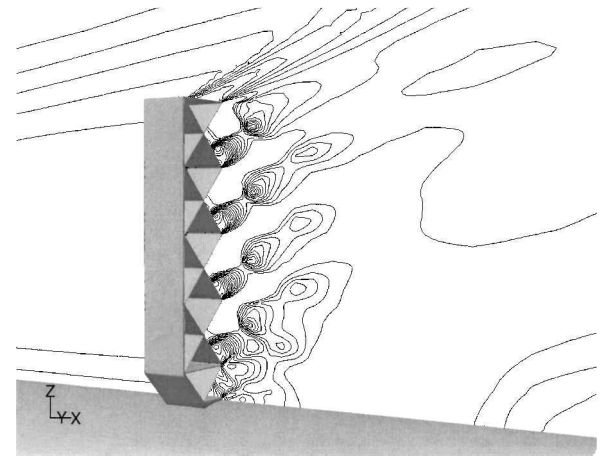

Fig. 14 Pressure coefficient contours on symmetry plane through leeward fin (fin 4); $\alpha = 20$ deg case.

cell from the top is at nearly a 0-deg α. At $\alpha = 20$ deg (Fig. 14), the entire leeward fin is at an effective negative α. This flow structure is responsible for the negative normal forces observed on the leeward fin in wind-tunnel tests and these calculations (see Fig. 10).

Conclusions

Calculations of the viscous flow past a missile with grid fins were made using CFD simulations. Comparing the computed aerodynamic coefficients for the missile and individual grid fins against detailed wind-tunnel measurement data validated the results. The validation process also included calculating the flowfield for the missile body alone and with conventional planar fins. Very good agreement with the measured data was observed for all configurations investigated. For the grid fin case, the aerodynamic coefficients were within 6.6% of the wind-tunnel data. The normal force coefficients on the individual grid fins were within 11% of the test data. The simulations were also successful in predicting the nonlinear behavior of the normal force on the leeward fin at the higher angles of attack. The physical nature of this effect was illustrated by presenting C_p contours on the symmetry plane through the leeward grid fin.

The viscous component of the axial force on the grid fin was about 1.5 times greater than that on the planar fin. This contrasts previous speculation that the smaller chord of the grid fin would result in less viscous force than a planar fin. The total axial force on an individual grid fin was about 2–3 times greater than that on the planar fin. As a percentage of the total force, the viscous component was about 16% for the grid fin, as compared to about 30% for the planar fin.

Results for inviscid calculations of the grid fin case were also presented. The normal force and pitching moment coefficients were calculated to within 11% of the experimental data. The Cartesian mesh generator, CART3D, significantly reduced the time required for mesh generation, even for the complicated grid fin geometry.

The investigation detailed in this paper demonstrated an approach for using viscous CFD simulations to calculate the flowfield and aerodynamic coefficients for a missile with grid fins. An unstructured mesh and wall functions were used to reduce the mesh size and computational requirements, but substantial computing resources were required. A viable alternative approach would be to use the chimera overset grid technique to generate a structured mesh. However, the nature of the grid fin design makes the required resources large, regardless of the approach used.

Acknowledgments

This work was supported in part by a grant of computer time from the U.S. Department of Defense High Performance Computing Modernization Program at the U.S. Army Research Laboratory Major Shared Resource Center, Aberdeen Proving Ground, Maryland. The authors would like to thank Graham Simpson and Anthony Sadler of the Defence Evaluation and Research Agency, United Kingdom, for providing the missile geometry and comprehensive database of wind-tunnel test data. Thanks are also due to support engineers at Fluent, Inc., for insight on approaches for mesh generation of the grid fin configuration. The authors also thank Michael Aftosmis, NASA Ames Research Center, California for providing additional inviscid simulations and discussions.

References

[1]Simpson, G. M., and Sadler, A. J., "Lattice Controls: A Comparison with Conventional, Planar Fins," *Proceedings of the NATO RTO Applied Vehicle Technology Panel Symposium on Missile Aerodynamics*, RTO-MP-5, NATO Research and Technology Organization, 1998, pp. (9-1)–(9-10).

[2]Washington, W. D., and Miller, M. S., "Experimental Investigations of Grid Fin Aerodynamics: A Synopsis of Nine Wind Tunnel and Three Flight Tests," *Proceedings of the NATO RTO Applied Vehicle Technology Panel Symposium on Missile Aerodynamics*, RTO-MP-5, NATO Research and Technology Organization, 1998, pp. (10-1)–(10-14).

[3]Miller, M. S., and Washington, W. D., "An Experimental Investigation of Grid Fin Drag Reduction Techniques," *Proceedings of the AIAA 12th Applied Aerodynamics Conference*, AIAA, Washington, DC, 1994, pp. 800–808.

[4]Washington, W. D., and Miller, M. S., "Grid Fins: A New Concept for Missile Stability and Control," AIAA Paper 93-0035, Jan. 1993.

[5]Abate, G., Duckerschein, R., and Hathaway, W., "Subsonic/Transonic Free-Flight Tests of a Generic Missile With Grid Fins," AIAA Paper 2000-0937, Jan. 2000.

[6]Kretzschmar, R. W., and Burkhalter, J. E., "Aerodynamic Prediction Methodology for Grid Fins," *Proceedings of the NATO RTO Applied Vehicle Technology Panel Symposium on Missile Aerodynamics*, RTO-MP-5, NATO Research and Technology Organization, 1998, pp. (11-1)–(11-11).

[7]Burkhalter, J. E., "Grid Fins for Missile Applications in Supersonic Flow," AIAA Paper 96-0194, Jan. 1996.

[8]Tong, Z., Lu, Z., and Shen, X., "Calculation and Analysis of Grid Fin Configurations," *Advances in Astronautical Sciences*, Vol. 91, 1996, pp. 1017–1023.

[9]Burkhalter, J. E., and Frank, H. M., "Grid Fin Aerodynamics for Missile Applications in Subsonic Flow," *Journal of Spacecraft and Rockets*, Vol. 33, No. 1, 1996, pp. 38–44.

[10]Burkhalter, J. E., Hartfield, R. J., and Leleux, T. M., "Nonlinear Aerodynamic Analysis of Grid Fin Configurations," *Journal of Aircraft*, Vol. 32, No. 3, 1995, pp. 547–554.

[11]Khalid, M., Sun, Y., and Xu, H., "Computation of Flows Past Grid Fin Missiles," *Proceedings of the NATO RTO Applied Vehicle Technology Panel Symposium on Missile Aerodynamics*, RTO-MP-5, NATO Research and Technology Organization, 1998, pp. (12-1)–(12-11).

[12]Sun, Y., and Khalid, M., "A CFD Investigation of Grid Fin Missiles," AIAA Paper 98-3571, July 1998.

[13]Lesage, F., "Numerical Investigation of the Supersonic Flow Inside a Grid Fin Cell," *Proceedings of the 17th International Symposium on Ballistics*, Vol. 1, American Defense Preparedness Association, Arlington, VA, 1998, pp. 209–216.

[14]Chen, S., Khalid, M., and Xu, H., "Comprehensive CFD Investigation of Grid Fins as Efficient Control Surface Devices," AIAA Paper 2000-0987, Jan. 2000.

[15]Spalart, P. R., and Allmaras, S. R., "One-Equation Turbulence Model for Aerodynamic Flows," AIAA Paper 92-0439, Jan. 1992.

[16]*Fluent 5.0 Users Guide*, Vol. 2, Fluent, Inc., Lebanon, NH, 1998.

[17]Edge, H. L., Sahu, J., Sturek, W. B., Pressel, D. M., Heavey, K. R., Weinacht, P., Zoltani, C. K., Nietubicz, C. J., Clarke, J., Behr, M., and Collins, P., "Common High Performance Computing Software Support Initiative (CHSSI) Computational Fluid Dynamics (CFD)-6 Project Final Report: ARL Block-Structured Gridding Zonal Navier–Stokes Flow (ZNSFLOW) Solver," U.S. Army Research Lab., Rept. ARL-TR-2084, Aberdeen Proving Ground, MD, Feb. 2000.

[18]Steger, J. L., and Warming, R. F., "Flux Vector Splitting of the Inviscid Gasdynamic Equations with Application to Finite-Difference Methods," *Journal of Computational Physics*, Vol. 40, No. 2, 1981, pp. 263–293.

[19]Ying, S. X., Steger, J. L., Schiff, L. B., and Baganoff, D., "Numerical Simulation of Unsteady, Viscous, High-Angle-of-Attack Flows Using a Partially Flux-Split Algorithm," AIAA Paper 86-2179, Aug. 1986.

[20]Sahu, J., "Numerical Simulation of Three-Dimensional Transonic Flows," *International Journal for Numerical Methods in Fluids*, Vol. 10, No. 8, 1990, pp. 855–873.

[21]Steger, J. L., Dougherty, F. C., and Benek, J. A., "A Chimera Grid Scheme," *Advances in Grid Generation*, edited by K. N. Ghia and U. Ghia, ASME FED-5, American Society of Mechanical Engineers, New York, 1983, pp. 59–69.

[22]Melton, J. E., "Automated Three-Dimensional Cartesian Grid Generation and Euler Flow Solutions for Arbitrary Geometries," Ph.D. Dissertation, Dept. of Mechanical and Aeronautical Engineering, Univ. California, Davis, CA, June 1996.

[23]Melton, J. E., Berger, M. J., Aftosmis, M. J., and Wong, M. D., "Three-Dimensional Applications of a Cartesian Grid Euler Method," AIAA Paper 95-0853, Jan. 1995.

[24]Aftosmis, M. J., Berger, M. J., and Melton, J. E., "Robust and Efficient Cartesian Mesh Generation for Component-Based Geometry," *AIAA Journal*, Vol. 36, No. 6, 1998, pp. 952–960.

[25]Aftosmis, M. J., "Solution Adaptive Cartesian Grid Methods for Aerodynamic Flows with Complex Geometries," *28th Computational Fluid Dynamics*, VKI LS 1997-02, von Kármán Inst. for Fluid Dynamics, Brussels, 1997, pp. 1–105.

[26]Aftosmis, M. J., Berger, M. J., and Adomavicius, G., "A Parallel Multilevel Method for Adaptively Refined Cartesian Grids with Embedded Boundaries," AIAA Paper 2000-0808, Jan. 2000.

P. Weinacht
Associate Editor